ATLAS CONF Note

ATLAS-CONF-2019-032

15th July 2019

Combined measurement of the total and differential cross sections in the $H \to \gamma\gamma$ and the $H \to ZZ^* \to 4\ell$ decay channels at $\sqrt{s} = 13$ TeV with the ATLAS detector

The ATLAS Collaboration

Combined measurements of the total and differential cross sections of Higgs boson production are performed with proton-proton collisions recorded by the ATLAS detector at the Large Hadron Collider. The data correspond to an integrated luminosity of 139 fb^{-1} produced at a center-of-mass energy of 13 TeV. The cross sections are obtained from the measured $H \to ZZ^* \to 4\ell$ and $H \to \gamma\gamma$ event yields, which are combined accounting for luminosity, detector effects, acceptances, and branching fractions. The measured total Higgs boson production cross section is $55.4^{+4.3}_{-4.2}$ pb, in agreement with the Standard Model prediction. A differential cross-section measurement is also performed as a function of the Higgs boson transverse momentum. The results from the two decay channels are found to be compatible with each other, and their combination agrees with the Standard Model predictions.

ATLAS-CONF-2019-032
15 July 2019

1 Introduction and methods

This note presents measurements of the total Higgs boson production cross section and of the differential cross section as a function of Higgs boson transverse momentum $p_{\mathrm{T,H}}$ using the $H \to \gamma\gamma$ and $H \to ZZ^* \to 4\ell$ (where $\ell = e, \mu$ throughout this note) final states. The results are obtained from the full Run-2 13 TeV proton-proton dataset, produced at the Large Hadron Collider (LHC), recorded by the ATLAS detector [1], and corresponding to an integrated luminosity of 139.0±2.4 fb^{-1} [2, 3]. The measurements are extrapolated to the full phase space and the measured cross sections are compared to Standard Model (SM) predictions.

Both the ATLAS and CMS collaborations have previously measured fiducial, total, and differential Higgs boson production cross sections in the $H \to \gamma\gamma$, $H \to ZZ^* \to 4\ell$, $H \to WW^* \to e\nu\mu\nu$, and $H \to b\bar{b}$ decay channels [4–11].

Full descriptions of the measurement of the event yields in the $H \to \gamma\gamma$ and $H \to ZZ^* \to 4\ell$ decay channels are given in Refs. [12, 13]. Corrections are applied to these yields accounting for luminosity, detector effects, fiducial acceptances, and branching fractions. The SM values of the Higgs boson branching fractions are used, and the acceptances are based on SM predictions. Uncertainties due to the model dependence of the acceptance factors are evaluated by varying the contribution of the different Higgs boson production modes. The value of the Higgs boson mass is assumed to be 125.09 GeV [14]. The combined differential cross-section measurement reported here is based on results obtained in the individual channels using bin-by-bin correction factors.

Details about the simulated events used for the calculation of the acceptance factors and the SM predictions can be found in Refs. [12, 13]. The gluon fusion (ggF) distributions are obtained using POWHEG NNLOPS [15–25], while other production mode distributions are simulated with POWHEG [15–17] except for $b\bar{b}H$ and tH, which are simulated using MG5_aMC@NLO [26, 27]. The samples are normalized to cross sections obtained from the best available predictions as provided by the LHC Higgs Cross Section Working Group [28]. Details on the cross-section predictions are given in Table 1, including the order of the calculations in both QCD and electroweak (EW) processes, and the SM composition of the production modes. N^{3}LO is an abbreviation for next-to-next-to-next-to-leading order.

Table 1: Cross-section predictions used to normalize simulated SM events for the ggF [29–39], VBF [40–42], VH [43–52], $t\bar{t}H$ [53–56], tH [57, 58], and $b\bar{b}H$ [59–61] production modes, with the accuracy of the calculation for both QCD and EW processes (if the latter is not mentioned, no EW corrections are applied) and the SM fraction of each production mode.

Process	Accuracy	Fraction [%]
ggF	N^{3}LO in QCD, NLO in EW	87.2
VBF	(approximate) NNLO in QCD, NLO in EW	6.8
VH	qq/qg: NNLO in QCD, NLO in EW; gg: NLO+NLL in QCD	4.0
$t\bar{t}H + tH$	$t\bar{t}H$: NLO in QCD, NLO in EW, tH: NLO in QCD	1.1
$b\bar{b}H$	NNLO (NLO) in QCD for 5FS (4FS)	0.9

The branching fraction for a Higgs boson with mass m_H = 125.09 GeV decaying to $H \to \gamma\gamma$ is predicted to be (0.227 ± 0.007)% [28], and the branching ratio to the four-lepton final state is predicted to be (0.0125 ± 0.0003)% [28]. Both branching ratios are calculated with HDECAY [62, 63] and PROPHECY4F [64, 65] and include the complete NLO QCD and EW corrections. In the $H \to ZZ^* \to 4\ell$ case, the interference effects between identical final-state fermions are included.

A likelihood combination of the two decay channels is performed, following the method described in Ref. [4]. The $p_{\mathrm{T,H}}$ binning in the $H \to \gamma\gamma$ analysis is finer than that in the $H \to ZZ^* \to 4\ell$ analysis. Where needed, the sum of the respective $H \to \gamma\gamma$ bins is combined with one $H \to ZZ^* \to 4\ell$ bin. Experimental and theoretical uncertainties that affect both channels are correlated by the implementation of common nuisance parameters. These include the uncertainties in the integrated luminosity, in the Higgs boson mass value, in the description of the pileup in the simulation, and in the contributions of the different Higgs boson production modes. Additionally, the uncertainties in the branching fractions are correlated through the correlation of the corresponding underlying sources. Finally, the uncertainties in the acceptance and correction factors due to variations of the modeling of the parton shower are also correlated. All other uncertainties are treated as uncorrelated. The asymptotic approximation [66] is used when computing the uncertainties in the cross-section measurements. The validity of this approximation has been verified in previous analyses by performing pseudo-experiments.

2 Results and Conclusion

The inclusive acceptance factors, relative to the full phase space, are about 50% for the $H \to \gamma\gamma$ channel and about 49% for the $H \to ZZ^* \to 4\ell$ channel. In the $H \to \gamma\gamma$ channel, the acceptance factor is about 50% at low $p_{\mathrm{T,H}}$, 45% at intermediate values, and about 75% at high $p_{\mathrm{T,H}}$. In the $H \to ZZ^* \to 4\ell$ channel, the acceptance factor varies from about 45% at low $p_{\mathrm{T,H}}$ to 65% at high $p_{\mathrm{T,H}}$.

The total Higgs boson production cross section is measured in the $H \to \gamma\gamma$ decay channel to be $56.7^{+6.4}_{-6.2}$ pb and in the $H \to ZZ^* \to 4\ell$ channel to be $54.4^{+5.6}_{-5.4}$ pb. Combining the two channels, a result of $55.4^{+4.3}_{-4.2}$ pb (± 3.1(stat.) $^{+3.0}_{-2.8}$(sys.)) is obtained. All three results are in agreement with the SM prediction of 55.6 ± 2.5 pb. Figure 1 shows the measured total cross section, together with the cross sections measured at $\sqrt{s} = 7$ and 8 TeV [67].

The differential cross sections as a function of $p_{\mathrm{T,H}}$ for the individual channels and their combination are shown in Figure 2, along with the SM prediction described above. The uncertainty band on the SM prediction includes PDF and α_S uncertainties as well as those due to missing higher-order corrections, obtained following the method described in Ref. [6]. The measurement uncertainty is dominated by the statistical component. The background modeling uncertainty in the $H \to \gamma\gamma$ analysis is the main source of systematic uncertainty, followed by the luminosity estimate.

The measurements in the two decay channels are found to be compatible with a p-value of 76% for the total cross section and 11% for the $p_{\mathrm{T,H}}$ distribution. The combined measurements are compatible with the SM predictions with a p-value of 96% for the total cross section and 78% for the $p_{\mathrm{T,H}}$ distribution. Both compatibility checks are performed using a likelihood approach, neglecting the uncertainties in the SM prediction.

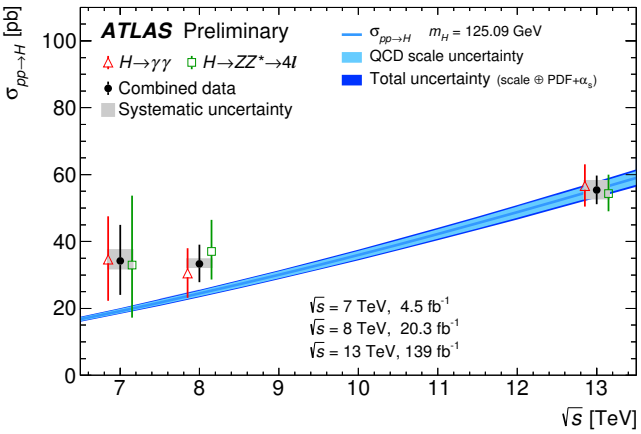

Figure 1: Total $pp \to H + X$ cross sections measured at center-of-mass energies of 7, 8, and 13 TeV, compared to Standard Model predictions. The $H \to \gamma\gamma$ channel (red triangles), $H \to ZZ^* \to 4\ell$ channel (green squares) and combined (black dots) measurements are shown. The individual channel results are offset along the x-axis for display purposes. The grey bands on the combined measurements represent the systematic uncertainty, while the error bars show the total uncertainty. The light blue band shows the estimated uncertainty due to missing higher-order corrections, and the dark blue band indicates the total uncertainty. The total theoretical uncertainty corresponds to the higher-order-correction uncertainty summed in quadrature with the sum of the PDF and α_S uncertainties, and is partially correlated across values of the center-of-mass energy.

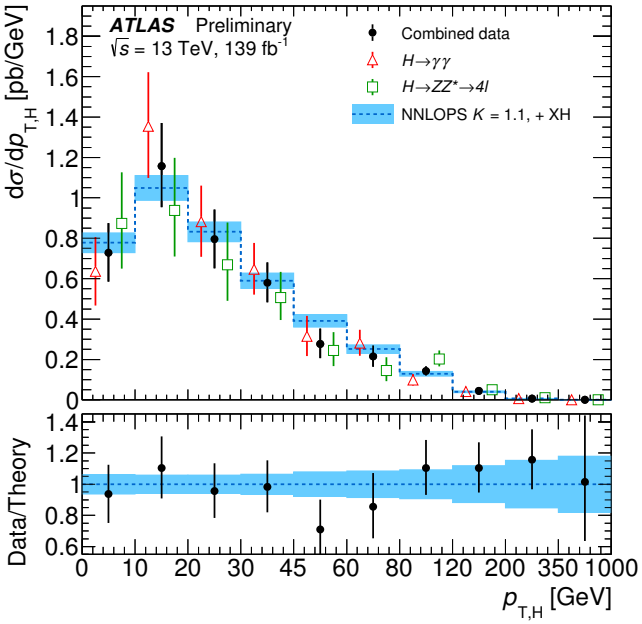

Figure 2: Differential $pp \to H + X$ cross section as a function of Higgs boson transverse momentum $p_{\mathrm{T,H}}$ in the full phase space, compared to Standard Model predictions. The $H \to \gamma\gamma$ (red triangles), $H \to ZZ^* \to 4\ell$ (green squares) and combined (black dots) measurements are shown. The blue dashed line shows the central value of the sum of the NNLOPS ggF prediction, scaled to the N^{3}LO prediction with a K-factor of 1.1, and the contribution of the other Higgs boson production modes XH. The SM prediction is overlaid with uncertainty bands including PDF and α_S uncertainties as well as those due to missing higher-order corrections. For better visibility, all bins are shown as having the same size, independent of their numerical width. The panel on the bottom shows the ratio of the combined measurement to the prediction.

Appendix

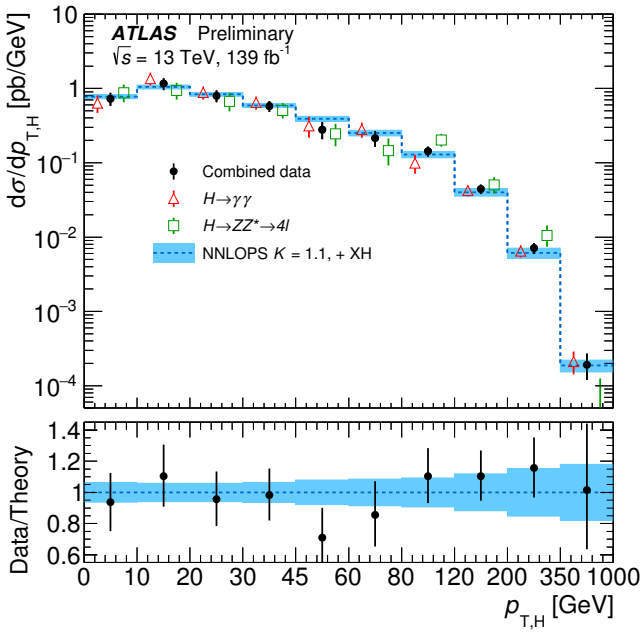

Figure 3: Differential $pp \to H + X$ cross section as a function of Higgs boson transverse momentum $p_{\mathrm{T,H}}$ in the full phase space, compared to Standard Model predictions. The $H \to \gamma\gamma$ (red triangles), $H \to ZZ^* \to 4\ell$ (green squares) and combined (black dots) measurements are shown. The blue dashed line shows the central value of the sum of the NNLOPS ggF prediction, scaled to the N^{3}LO prediction with a K-factor of 1.1, and the contribution of the other Higgs boson production modes XH. The SM prediction is overlaid with uncertainty bands including PDF and α_S uncertainties as well as those due to missing higher-order corrections. For better visibility, all bins are shown as having the same size, independent of their numerical width. The panel on the bottom shows the ratio of the combined measurement to the prediction.

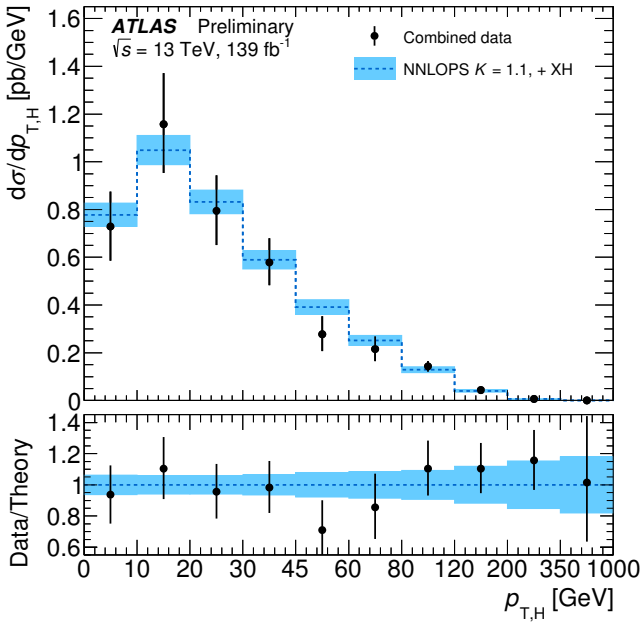

Figure 4: Combined measurement of the differential $pp \to H + X$ cross section as a function of Higgs boson transverse momentum $p_{\mathrm{T,H}}$ in the full phase space, compared to Standard Model predictions. The blue dashed line shows the central value of the sum of the NNLOPS ggF prediction, scaled to the N^{3}LO prediction with a K-factor of 1.1, and the contribution of the other Higgs boson production modes XH. The SM prediction is overlaid with uncertainty bands including PDF and α_S uncertainties as well as those due to missing higher-order corrections. For better visibility, all bins are shown as having the same size, independent of their numerical width. The panel on the bottom shows the ratio of the combined measurement to the prediction.

Table 2: Combined measurement of the differential $pp \to H + X$ cross section as a function of Higgs boson transverse momentum $p_{\mathrm{T,H}}$ in the full phase space.

$p_{\mathrm{T,H}}$ Bin	$d\sigma/dp_{\mathrm{T,H}}$ (pb/GeV)
0-10 GeV	0.73 ± 0.15
10-20 GeV	1.16 ± 0.21
20-30 GeV	0.80 ± 0.15
30-45 GeV	0.58 ± 0.10
45-60 GeV	0.278 ± 0.075
60-80 GeV	0.215 ± 0.054
80-120 GeV	0.142 ± 0.023
120-200 GeV	0.044 ± 0.007
200-350 GeV	0.007 ± 0.001
350-1000 GeV	$0.0002 \pm 8 \times 10^{-5}$

References

[1] ATLAS Collaboration, *The ATLAS Experiment at the CERN Large Hadron Collider*, JINST **3** (2008) S08003 (cit. on p. 2).

[2] ATLAS Collaboration, *Luminosity determination in pp collisions at $\sqrt{s}$ = 13 TeV using the ATLAS detector at the LHC*, ATLAS-CONF-2019-021, 2019, URL: https://cds.cern.ch/record/2677054 (cit. on p. 2).

[3] G. Avoni et al., *The new LUCID-2 detector for luminosity measurement and monitoring in ATLAS*, JINST **13** (2018) P07017 (cit. on p. 2).

[4] ATLAS Collaboration, *Combined measurement of differential and total cross sections in the $H \to \gamma\gamma$ and the $H \to ZZ^* \to 4\ell$ decay channels at $\sqrt{s}$ = 13 TeV with the ATLAS detector*, Phys. Lett. B **786** (2018) 114, arXiv: 1805.10197 [hep-ex] (cit. on pp. 2, 3).

[5] ATLAS Collaboration, *Measurement of inclusive and differential cross sections in the $H \to ZZ^* \to 4\ell$ decay channel in pp collisions at $\sqrt{s}$ = 13 TeV with the ATLAS detector*, JHEP **10** (2017) 132, arXiv: 1708.02810 [hep-ex] (cit. on p. 2).

[6] ATLAS Collaboration, *Measurements of Higgs boson properties in the diphoton decay channel with 36 fb^{-1} of pp collision data at $\sqrt{s}$ = 13 TeV with the ATLAS detector*, Phys. Rev. D **98** (2018) 052005, arXiv: 1802.04146 [hep-ex] (cit. on pp. 2, 3).

[7] ATLAS Collaboration, *Measurements of gluon-gluon fusion and vector-boson fusion Higgs boson production cross-sections in the $H \to WW^* \to e\nu\mu\nu$ decay channel in pp collisions at $\sqrt{s}$ = 13 TeV with the ATLAS detector*, Phys. Lett. B **789** (2019) 508, arXiv: 1808.09054 [hep-ex] (cit. on p. 2).

[8] CMS Collaboration, *Measurement and interpretation of differential cross sections for Higgs boson production at $\sqrt{s}$ = 13 TeV*, Phys. Lett. (2018), arXiv: 1812.06504 [hep-ex] (cit. on p. 2).

[9] CMS Collaboration, *Measurement of inclusive and differential Higgs boson production cross sections in the diphoton decay channel in proton–proton collisions at $\sqrt{s}$ = 13 TeV*, JHEP **01** (2019) 183, arXiv: 1807.03825 [hep-ex] (cit. on p. 2).

[10] CMS Collaboration, *Measurements of properties of the Higgs boson decaying into the four-lepton final state in pp collisions at $\sqrt{s}$ = 13 TeV*, JHEP **11** (2017) 047, arXiv: 1706.09936 [hep-ex] (cit. on p. 2).

[11] CMS Collaboration, *Measurement of the transverse momentum spectrum of the Higgs boson produced in pp collisions at $\sqrt{s}$ = 8 TeV using $H \to WW$ decays*, JHEP **03** (2017) 032, arXiv: 1606.01522 [hep-ex] (cit. on p. 2).

[12] ATLAS Collaboration, *Measurements of the Higgs boson inclusive, differential and production cross sections in the 4ℓ decay channel at $\sqrt{s}$ = 13 TeV with the ATLAS detector*, ATLAS-CONF-2019-025, 2019, URL: http://cdsweb.cern.ch/record/2682107 (cit. on p. 2).

[13] ATLAS Collaboration, *Measurements and interpretations of Higgs-boson fiducial cross sections in the diphoton decay channel using 139 fb^{-1} of pp collision data at $\sqrt{s}$ = 13 TeV with the ATLAS detector*, ATLAS-CONF-2019-029, 2019, URL: https://cds.cern.ch/record/2682800 (cit. on p. 2).

[14] ATLAS and CMS Collaborations, *Combined Measurement of the Higgs Boson Mass in pp Collisions at $\sqrt{s}$ = 7 and 8 TeV with the ATLAS and CMS Experiments*, Phys. Rev. Lett. **114** (2015) 191803, arXiv: 1503.07589 [hep-ex] (cit. on p. 2).

[15] P. Nason, *A New method for combining NLO QCD with shower Monte Carlo algorithms*, JHEP **11** (2004) 040, arXiv: hep-ph/0409146 (cit. on p. 2).

[16] S. Frixione, P. Nason and C. Oleari, *Matching NLO QCD computations with parton shower simulations: the POWHEG method*, JHEP **11** (2007) 070, arXiv: 0709.2092 [hep-ph] (cit. on p. 2).

[17] S. Alioli, P. Nason, C. Oleari and E. Re, *A general framework for implementing NLO calculations in shower Monte Carlo programs: the POWHEG BOX*, JHEP **06** (2010) 043, arXiv: 1002.2581 [hep-ph] (cit. on p. 2).

[18] K. Hamilton, P. Nason, E. Re and G. Zanderighi, *NNLOPS simulation of Higgs boson production*, JHEP **10** (2013) 222, arXiv: 1309.0017 [hep-ph] (cit. on p. 2).

[19] K. Hamilton, P. Nason and G. Zanderighi, *Finite quark-mass effects in the NNLOPS POWHEG+MiNLO Higgs generator*, JHEP **05** (2015) 140, arXiv: 1501.04637 [hep-ph] (cit. on p. 2).

[20] K. Hamilton, P. Nason and G. Zanderighi, *MINLO: Multi-Scale Improved NLO*, JHEP **10** (2012) 155, arXiv: 1206.3572 [hep-ph] (cit. on p. 2).

[21] J. M. Campbell et al., *NLO Higgs Boson Production Plus One and Two Jets Using the POWHEG BOX, MadGraph4 and MCFM*, JHEP **07** (2012) 092, arXiv: 1202.5475 [hep-ph] (cit. on p. 2).

[22] K. Hamilton, P. Nason, C. Oleari and G. Zanderighi, *Merging H/W/Z + 0 and 1 jet at NLO with no merging scale: a path to parton shower + NNLO matching*, JHEP **05** (2013) 082, arXiv: 1212.4504 [hep-ph] (cit. on p. 2).

[23] S. Catani and M. Grazzini, *An NNLO subtraction formalism in hadron collisions and its application to Higgs boson production at the LHC*, Phys. Rev. Lett. **98** (2007) 222002, arXiv: hep-ph/0703012 [hep-ph] (cit. on p. 2).

[24] G. Bozzi, S. Catani, de Florian Daniel and M. Grazzini, *Transverse-momentum resummation and the spectrum of the Higgs boson at the LHC*, Nucl. Phys. **B737** (2006) 73, arXiv: hep-ph/0508068 [hep-ph] (cit. on p. 2).

[25] D. de Florian, G. Ferrera, M. Grazzini and D. Tommasini, *Transverse-momentum resummation: Higgs boson production at the Tevatron and the LHC*, JHEP **11** (2011) 064, arXiv: 1109.2109 [hep-ph] (cit. on p. 2).

[26] J. Alwall et al., *The automated computation of tree-level and next-to-leading order differential cross sections, and their matching to parton shower simulations*, JHEP **07** (2014) 079, arXiv: 1405.0301 [hep-ph] (cit. on p. 2).

[27] M. Wiesemann et al., *Higgs production in association with bottom quarks*, JHEP **02** (2015) 132, arXiv: 1409.5301 [hep-ph] (cit. on p. 2).

[28] D. de Florian et al., *Handbook of LHC Higgs Cross Sections: 4. Deciphering the Nature of the Higgs Sector*, 2016, arXiv: 1610.07922 [hep-ph] (cit. on p. 2).

[29] C. Anastasiou et al., *High precision determination of the gluon fusion Higgs boson cross-section at the LHC*, JHEP **05** (2016) 058, arXiv: 1602.00695 [hep-ph] (cit. on p. 2).

[30] C. Anastasiou, C. Duhr, F. Dulat, F. Herzog and B. Mistlberger, *Higgs Boson Gluon-Fusion Production in QCD at Three Loops*, Phys. Rev. Lett. **114** (2015) 212001, arXiv: 1503.06056 [hep-ph] (cit. on p. 2).

[31] F. Dulat, A. Lazopoulos and B. Mistlberger, *iHixs 2 – Inclusive Higgs cross sections*, Comput. Phys. Commun. **233** (2018) 243, arXiv: 1802.00827 [hep-ph] (cit. on p. 2).

[32] R. V. Harlander and K. J. Ozeren, *Finite top mass effects for hadronic Higgs production at next-to-next-to-leading order*, JHEP **11** (2009) 088, arXiv: 0909.3420 [hep-ph] (cit. on p. 2).

[33] R. V. Harlander and K. J. Ozeren, *Top mass effects in Higgs production at next-to-next-to-leading order QCD: Virtual corrections*, Phys. Lett. **B679** (2009) 467, arXiv: 0907.2997 [hep-ph] (cit. on p. 2).

[34] R. V. Harlander, H. Mantler, S. Marzani and K. J. Ozeren, *Higgs production in gluon fusion at next-to-next-to-leading order QCD for finite top mass*, Eur. Phys. J. **C66** (2010) 359, arXiv: 0912.2104 [hep-ph] (cit. on p. 2).

[35] A. Pak, M. Rogal and M. Steinhauser, *Finite top quark mass effects in NNLO Higgs boson production at LHC*, JHEP **02** (2010) 025, arXiv: 0911.4662 [hep-ph] (cit. on p. 2).

[36] S. Actis, G. Passarino, C. Sturm and S. Uccirati, *NLO Electroweak Corrections to Higgs Boson Production at Hadron Colliders*, Phys. Lett. **B670** (2008) 12, arXiv: 0809.1301 [hep-ph] (cit. on p. 2).

[37] S. Actis, G. Passarino, C. Sturm and S. Uccirati, *NNLO Computational Techniques: The Cases $H \to \gamma\gamma$ and $H \to gg$*, Nucl. Phys. **B811** (2009) 182, arXiv: 0809.3667 [hep-ph] (cit. on p. 2).

[38] M. Bonetti, K. Melnikov and L. Tancredi, *Higher order corrections to mixed QCD-EW contributions to Higgs boson production in gluon fusion*, Phys. Rev. **D97** (2018) 056017, [Erratum: Phys. Rev.D97,no.9,099906(2018)], arXiv: 1801.10403 [hep-ph] (cit. on p. 2).

[39] U. Aglietti, R. Bonciani, G. Degrassi and A. Vicini, *Two loop light fermion contribution to Higgs production and decays*, Phys. Lett. **B595** (2004) 432, arXiv: hep-ph/0404071 [hep-ph] (cit. on p. 2).

[40] M. Ciccolini, A. Denner and S. Dittmaier, *Strong and electroweak corrections to the production of Higgs + 2jets via weak interactions at the LHC*, Phys. Rev. Lett. **99** (2007) 161803, arXiv: 0707.0381 [hep-ph] (cit. on p. 2).

[41] M. Ciccolini, A. Denner and S. Dittmaier, *Electroweak and QCD corrections to Higgs production via vector-boson fusion at the LHC*, Phys. Rev. **D77** (2008) 013002, arXiv: 0710.4749 [hep-ph] (cit. on p. 2).

[42] P. Bolzoni, F. Maltoni, S.-O. Moch and M. Zaro, *Higgs production via vector-boson fusion at NNLO in QCD*, Phys. Rev. Lett. **105** (2010) 011801, arXiv: 1003.4451 [hep-ph] (cit. on p. 2).

[43] O. Brein, R. V. Harlander and T. J. E. Zirke, *vh@nnlo - Higgs Strahlung at hadron colliders*, Comput. Phys. Commun. **184** (2013) 998, arXiv: 1210.5347 [hep-ph] (cit. on p. 2).

[44] R. V. Harlander, J. Klappert, S. Liebler and L. Simon, *vh@nnlo-v2: New physics in Higgs Strahlung*, JHEP **05** (2018) 089, arXiv: 1802.04817 [hep-ph] (cit. on p. 2).

[45] O. Brein, A. Djouadi and R. Harlander, *NNLO QCD corrections to the Higgs-strahlung processes at hadron colliders*, Phys. Lett. **B579** (2004) 149, arXiv: hep-ph/0307206 [hep-ph] (cit. on p. 2).

[46] O. Brein, R. Harlander, M. Wiesemann and T. Zirke, *Top-Quark Mediated Effects in Hadronic Higgs-Strahlung*, Eur. Phys. J. **C72** (2012) 1868, arXiv: 1111.0761 [hep-ph] (cit. on p. 2).

[47] L. Altenkamp, S. Dittmaier, R. V. Harlander, H. Rzehak and T. J. E. Zirke, *Gluon-induced Higgs-strahlung at next-to-leading order QCD*, JHEP **02** (2013) 078, arXiv: 1211.5015 [hep-ph] (cit. on p. 2).

[48] R. V. Harlander, A. Kulesza, V. Theeuwes and T. Zirke, *Soft gluon resummation for gluon-induced Higgs Strahlung*, JHEP **11** (2014) 082, arXiv: 1410.0217 [hep-ph] (cit. on p. 2).

[49] A. Denner, S. Dittmaier, S. Kallweit and A. Mück, *HAWK 2.0: A Monte Carlo program for Higgs production in vector-boson fusion and Higgs strahlung at hadron colliders*, Comput. Phys. Commun. **195** (2015) 161, arXiv: 1412.5390 [hep-ph] (cit. on p. 2).

[50] M. L. Ciccolini, S. Dittmaier and M. Kramer, *Electroweak radiative corrections to associated WH and ZH production at hadron colliders*, Phys. Rev. **D68** (2003) 073003, arXiv: hep-ph/0306234 [hep-ph] (cit. on p. 2).

[51] G. Ferrera, G. Somogyi and F. Tramontano, *Associated production of a Higgs boson decaying into bottom quarks at the LHC in full NNLO QCD*, Phys. Lett. **B780** (2018) 346, arXiv: 1705.10304 [hep-ph] (cit. on p. 2).

[52] F. Caola, G. Luisoni, K. Melnikov and R. Röntsch, *NNLO QCD corrections to associated WH production and $H \to b\bar{b}$ decay*, Phys. Rev. **D97** (2018) 074022, arXiv: 1712.06954 [hep-ph] (cit. on p. 2).

[53] W. Beenakker et al., *NLO QCD corrections to t anti-t H production in hadron collisions*, Nucl. Phys. **B653** (2003) 151, arXiv: hep-ph/0211352 [hep-ph] (cit. on p. 2).

[54] S. Dawson, C. Jackson, L. H. Orr, L. Reina and D. Wackeroth, *Associated Higgs production with top quarks at the large hadron collider: NLO QCD corrections*, Phys. Rev. **D68** (2003) 034022, arXiv: hep-ph/0305087 [hep-ph] (cit. on p. 2).

[55] Y. Zhang, W.-G. Ma, R.-Y. Zhang, C. Chen and L. Guo, *QCD NLO and EW NLO corrections to $t\bar{t}H$ production with top quark decays at hadron collider*, Phys. Lett. **B738** (2014) 1, arXiv: 1407.1110 [hep-ph] (cit. on p. 2).

[56] S. Frixione, V. Hirschi, D. Pagani, H.-S. Shao and M. Zaro, *Electroweak and QCD corrections to top-pair hadroproduction in association with heavy bosons*, JHEP **06** (2015) 184, arXiv: 1504.03446 [hep-ph] (cit. on p. 2).

[57] F. Demartin, F. Maltoni, K. Mawatari and M. Zaro, *Higgs production in association with a single top quark at the LHC*, Eur. Phys. J. **C75** (2015) 267, arXiv: 1504.00611 [hep-ph] (cit. on p. 2).

[58] F. Demartin, B. Maier, F. Maltoni, K. Mawatari and M. Zaro, *tWH associated production at the LHC*, Eur. Phys. J. **C77** (2017) 34, arXiv: 1607.05862 [hep-ph] (cit. on p. 2).

[59] S. Dawson, C. B. Jackson, L. Reina and D. Wackeroth, *Exclusive Higgs boson production with bottom quarks at hadron colliders*, Phys. Rev. **D69** (2004) 074027, arXiv: hep-ph/0311067 [hep-ph] (cit. on p. 2).

[60] S. Dittmaier, M. Krämer and M. Spira, *Higgs radiation off bottom quarks at the Tevatron and the CERN LHC*, Phys. Rev. **D70** (2004) 074010, arXiv: hep-ph/0309204 [hep-ph] (cit. on p. 2).

[61] R. Harlander, M. Kramer and M. Schumacher, *Bottom-quark associated Higgs-boson production: reconciling the four- and five-flavour scheme approach*, (2011), arXiv: 1112.3478 [hep-ph] (cit. on p. 2).

[62] A. Djouadi, J. Kalinowski and M. Spira, *HDECAY: A Program for Higgs boson decays in the Standard Model and its supersymmetric extension*, Comput. Phys. Commun. **108** (1998) 56, arXiv: hep-ph/9704448 (cit. on p. 2).

[63] A. Djouadi, J. Kalinowski, M. Muehlleitner and M. Spira, *HDECAY: Twenty$_{++}$ Years After*, (2018), arXiv: 1801.09506 [hep-ph] (cit. on p. 2).

[64] A. Bredenstein, A. Denner, S. Dittmaier and M. Weber, *Precise predictions for the Higgs-boson decay $H \to WW/ZZ \to 4$ leptons*, Phys. Rev. D **74** (2006) 013004, arXiv: hep-ph/0604011 (cit. on p. 2).

[65] A. Bredenstein, A. Denner, S. Dittmaier and M. Weber, *Radiative corrections to the semileptonic and hadronic Higgs-boson decays $H \to WW/ZZ \to 4$ fermions*, JHEP **02** (2007) 080, arXiv: hep-ph/0611234 (cit. on p. 2).

[66] G. Cowan, K. Cranmer, E. Gross and O. Vitells, *Asymptotic formulae for likelihood-based tests of new physics*, Eur. Phys. J. C **71** (2011) 1554, arXiv: 1007.1727 [physics.data-an], Erratum: Eur. Phys. J. C **73** (2013) 2501 (cit. on p. 3).

[67] ATLAS Collaboration, *Measurements of the total cross sections for Higgs boson production combining the $H \to \gamma\gamma$ and $H \to ZZ^* \to 4\ell$ decay channels at 7, 8 and 13 TeV center-of-mass energies with the ATLAS detector*, ATLAS-CONF-2015-069, 2015, URL: https://cds.cern.ch/record/2114841 (cit. on p. 3).